Extended Data Figures and Legends:

Extended data Figures 1 to 10

1. **Intraoperative photographs and electrode co-registration with atlases.**
2. **Selective visual attention task.**
3. **Average coherence and GC influence spectra per monkey.**
4. **DAI-SLN correlation spectra for each task period.**
5. **Granger-causal influence spectra during post-cue period.**
6. **Granger-causal influence spectra during pre-cue period.**
7. **Granger-causal influence spectra during pre-stimulus period.**
8. **Granger-causal influence spectra per session and for CSDs.**
9. **Conditional Granger-causal influence spectra and resulting functional hierarchy.**
10. **Granger-causal influence spectra excluding microsaccade effects.**

Extended Data Figure 1 | Intraoperative photographs and electrode co-registration with atlases. a, Intraoperative photograph of the brain of monkey 1 after placement of the ECoG grid. **b**, Co-registration of the electrode positions with the 3D brain model derived from structural MRI. Lines indicate the boundary of the covered brain region and the major sulci, and dots indicate the 252 subdural electrodes. The electrodes were arranged in lanes. Those lanes ran medio-laterally over most of the covered region and posterio-anteriorally at the frontal end of the covered region. Furthermore, electrodes were recorded through eight 32-channel headstages. Electrodes recorded through the same headstage are shown in the same colour, and electrodes on alternating lanes in dark/light, such that electrodes of the same lane and recorded through the same headstage were given the same colour and darkness. Bipolar derivations were obtained for all pairs of immediately neighbouring electrodes on the same lane, which were also recorded through the same headstage. For the medio-laterally running lanes, the difference was [(lateral electrode) minus (medial electrode)]; for the posterior-anteriorly running lanes, the difference was [(anterior electrode) minus (posterior electrode)]. Bipolar derivations were used in the analysis only when both electrodes had been assigned to one and the same area, excluding pairs of electrodes that crossed area boundaries. As a control for the arbitrary absolute phases obtained from bipolar derivations, we also used a current-source density (CSD) approach. For each CSD site, three immediately neighbouring electrodes along a lane of electrodes were used, and the average signal of the two flanking electrodes was subtracted from the signal of the central electrode. The sequences of three electrodes were running medio-laterally or posterior-anteriorly, corresponding to the orientation of the respective lane. CSDs were assigned to the area in which the central electrode was located. If neighbouring areas shared an electrode in one of their CSDs, this CSD was excluded from the area with the larger number of electrodes when calculating coherence or GC influences between those areas. **c-f**, Midthickness surface of the brain coregistered in Caret (http://www.nitrc.org/projects/caret/) to the Macaque.F99 space and thereby to the following atlases: (**c**) “Felleman-VE all (1991)”, **d**, “PHT 00 (PaxinosEtAl)”, **e,** “Markov-CC10”, **f**, “Markov-CC12”. The visual areas that were covered by the ECoG grid are highlighted. **g-l**, Same as **a-f**, but for monkey 2. **m** same as Fig. 1b but for monkey 2.

Extended Data Figure 2 | Selective visual attention task. See Methods/Experimental paradigm for details.

Extended Data Figure 3 | Average coherence and GC influence spectra per monkey. a, b, For the two monkeys separately, all inter-areal coherence spectra were averaged, and peaks were found using an automatic peak-detecting algorithm. The resulting band definitions are indicated by grey bars. **c, d,** GC influence spectra averaged across all pairs of areas, separately for each animal, and for the bottom-up and top-down direction (as indicated by the colour legend). Hierarchical position of each area was determined based on the most recent anatomical hierarchical model of the visual system[4]. In monkey 1, coherence and GC influence values in the range from 45-55 Hz and 95-105 Hz are masked because of residual line noise. n.s. not significant, *** $p<0.001$.

Extended Data Figure 4 | DAI-SLN correlation spectra for each task period. Same as figure 2**b**, but for each task period separately. During the pre-stimulus period, the monkey was already fixating, but neither the stimuli nor the cue had been shown. During the pre-cue period, the stimuli were on, but the attentional cue had not yet been presented. The DAI-SLN correlation spectra for the pre-stimulus and pre-cue periods were similar to the post-cue spectrum. In particular, they also showed positive correlations for theta and gamma, and a negative correlation for beta.

Extended Data Figure 5 | Granger-causal influence spectra during post-cue period. Hierarchical position of each area was determined based on the most recent anatomical hierarchical model of the visual system[4]. Bottom-up GC influence spectra are depicted in green, top-down GC influence spectra in black. **a,** Average bottom-up and top-down GC influence spectra for each target area, as indicated on the top, during the post-cue period. For each target area separately the GC influences between that area’s sites and all other sites were averaged. GC influence spectra were sorted into bottom-up and top-down directions according to the most recent anatomical hierarchical model[4]. As the peak frequencies for the beta and gamma bands differed between monkeys, the respective peaks (determined as illustrated in Extended Date Fig. 3**a, b**) were aligned before averaging. **b,** Same as **a,** but for each area pair separately and including the coherence spectra in red. Blue lines indicate the 95th percentile of the bias distribution. The significance of the directional asymmetry is indicated per area pair: n.s. not significant, * $p<0.05$, ** $p<0.01$, *** $p<0.001$.

Extended Data Figure 6 | Granger-causal influence spectra during pre-cue period. Same as Extended Data Fig. 5, but for the pre-cue period.

Extended Data Figure 7 | Granger-causal influence spectra during pre-stimulus period. Same as Extended Data Fig. 5, but for the pre-stimulus period. The gamma band is omitted, because there was no gamma band peak in the pre-stimulus period.

Extended Data Figure 8 | Granger-causal influence spectra per session and for CSDs. a, b, GC influence spectra averaged across all pairs of areas, separately for each animal (**a**:

monkey 1, **b**: monkey 2), for each recording session (as indicated by the titles above each panel), and for the bottom-up and top-down direction (as indicated by the colour legend). Hierarchical position of each area was determined based on the most recent anatomical hierarchical model of the visual system[4]. The titles above each panel indicate the session number, the number of successfully completed trials, and the resulting number of post-cue 0.5 s epochs obtained in that session. The plots demonstrate the stability of the overall pattern over different recording sessions with their unavoidable variance in observation noise. Note that for observation noise to contribute to the observed differences between bottom-up and top-down GC influences[20], it would need to depend on hierarchical level in a band-specific way, namely increasing for theta and gamma and decreasing for beta, which is highly unlikely. **c, d,** Same as extended data figure 3**c, d,** but using current source density (CSD) instead of bipolar derivation. This demonstrates that the overall pattern is independent of the bipolar derivation scheme. n.s. not significant, * $p<0.05$, ** $p<0.01$, *** $p<0.001$.

Extended Data Figure 9 | Conditional Granger-causal influence spectra and resulting functional hierarchy. a, b, Same as extended data figure 3**c, d**, but after conditioning the GC influence between each area pair on all other areas. **c,** Same as figure 2**c**, but after conditioning the GC influence between each area pair on all other areas. **d,** Same as figure 3**a,** but after conditioning the GC influence between each area pair on all other areas. We considered that the GC influences between two areas might be fully or partly mediated through one or more of the other areas. To investigate this possibility, we calculated for each pair of areas the conditional GC influence spectra[21], taking all other areas into account (see Methods for details). In short, this left the pattern of results qualitatively unchanged for gamma and beta: After conditioning, the correlation between DAI and SLN was positive in the gamma band (R=0.36, p=0005) and negative in the beta band (R=-0.21, p=0.045), suggesting that the recorded areas influenced each other to a substantial degree directly. Whether this holds after taking additional areas into account will need to be tested through simultaneous recordings. For theta, conditioning rendered the correlation insignificant (p=0.89), suggesting that theta-mediated influences might involve larger networks. After conditioning, the DAI combined across frequency bands remained significantly correlated with SLN (**c**) and a hierarchy built on the pattern of conditional GC influences (**d**) was correlated to the anatomical hierarchy[4] (R=0.88, P=0.0072).

Extended Data Figure 10 | Granger-causal influence spectra excluding microsaccade effects. a, b, Same as extended data figure 3**c, d**, but for 0.5 s long data epochs without microsaccades and starting at least 0.3 s after microsaccades to avoid effects of LFP locking after microsaccades on the GC influence spectra. The numbers of data epochs fulfilling the criteria for this analysis are indicated above the panels. Please note that this approach excludes microsaccade effects in the beta and gamma bands, but not in the theta band.

Extended Data Figure 1

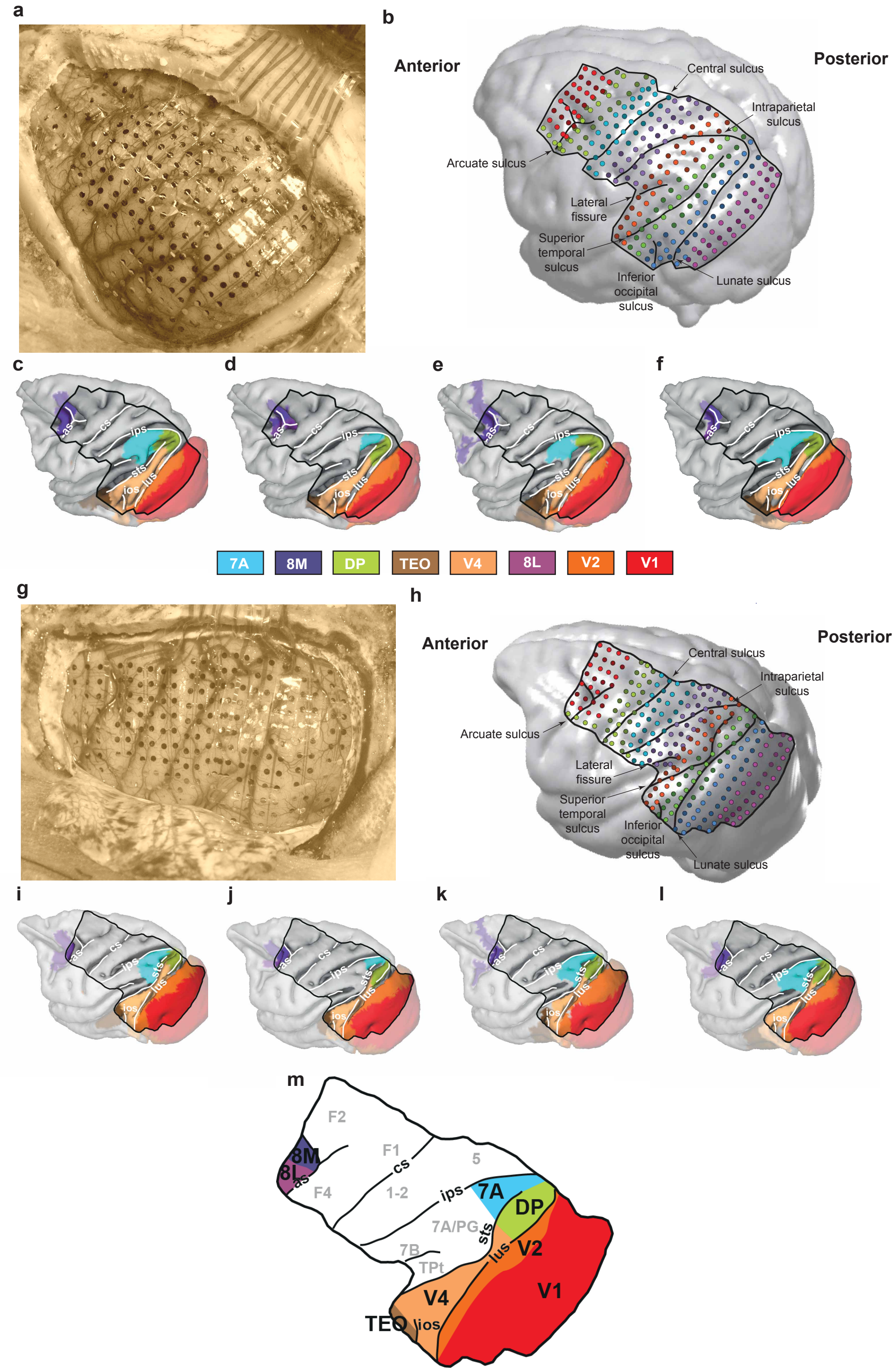

Extended Data Figure 2

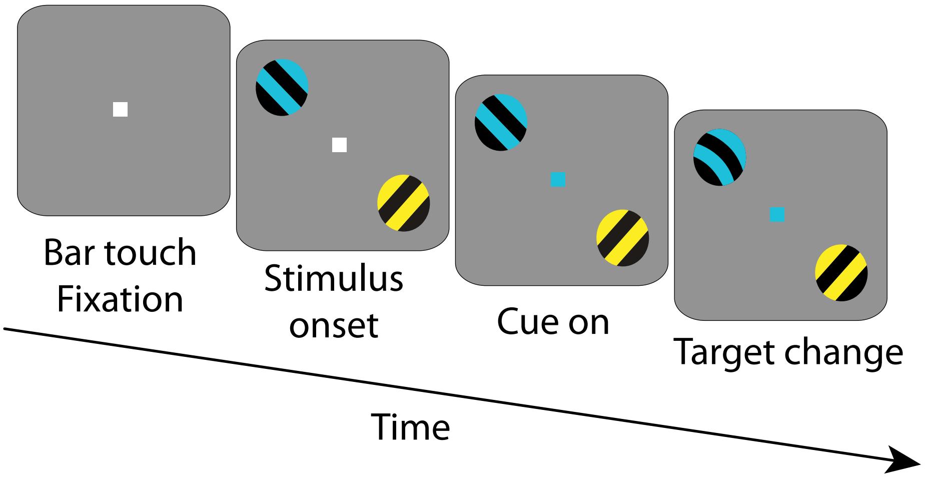

Extended Data Figure 3

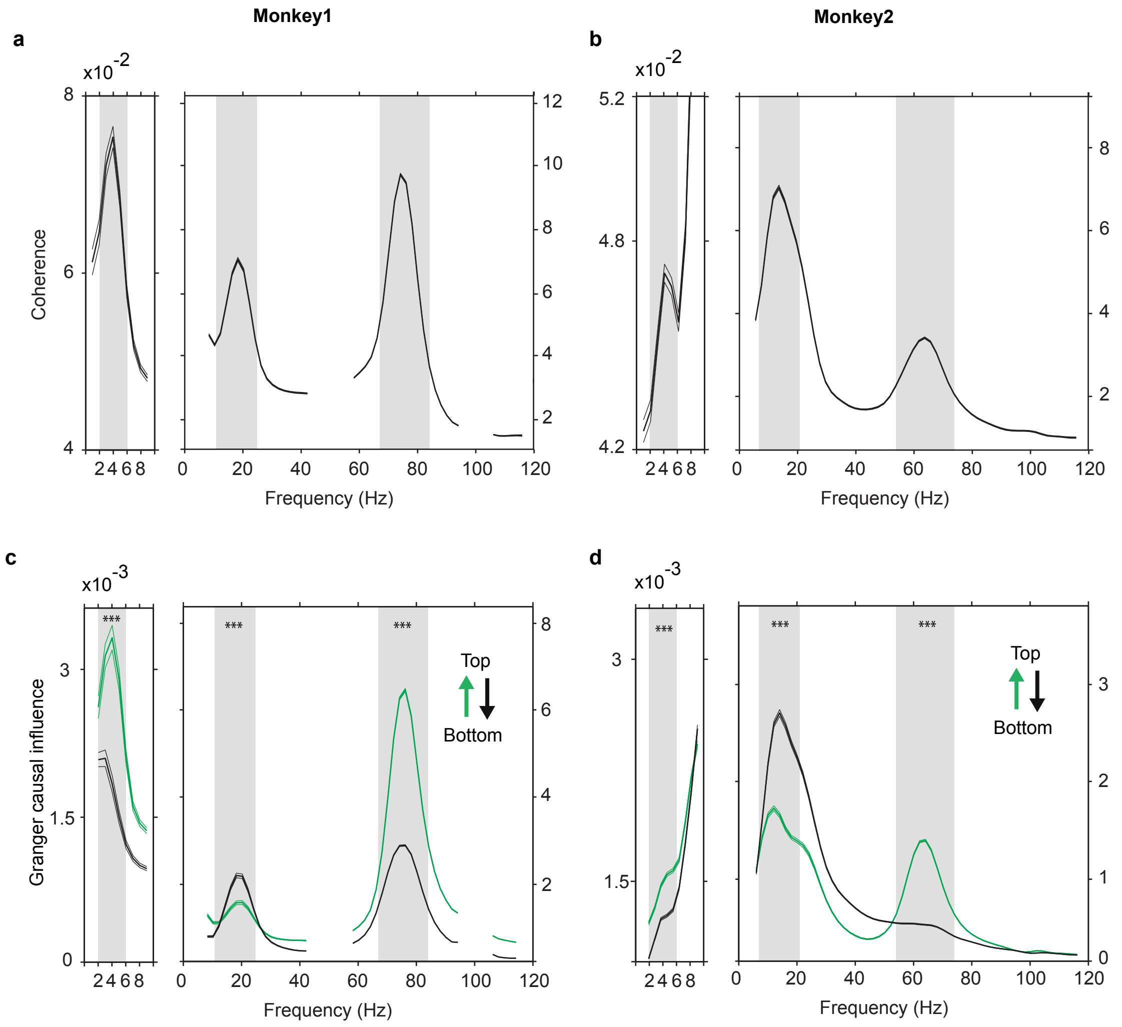

Extended Data Figure 4

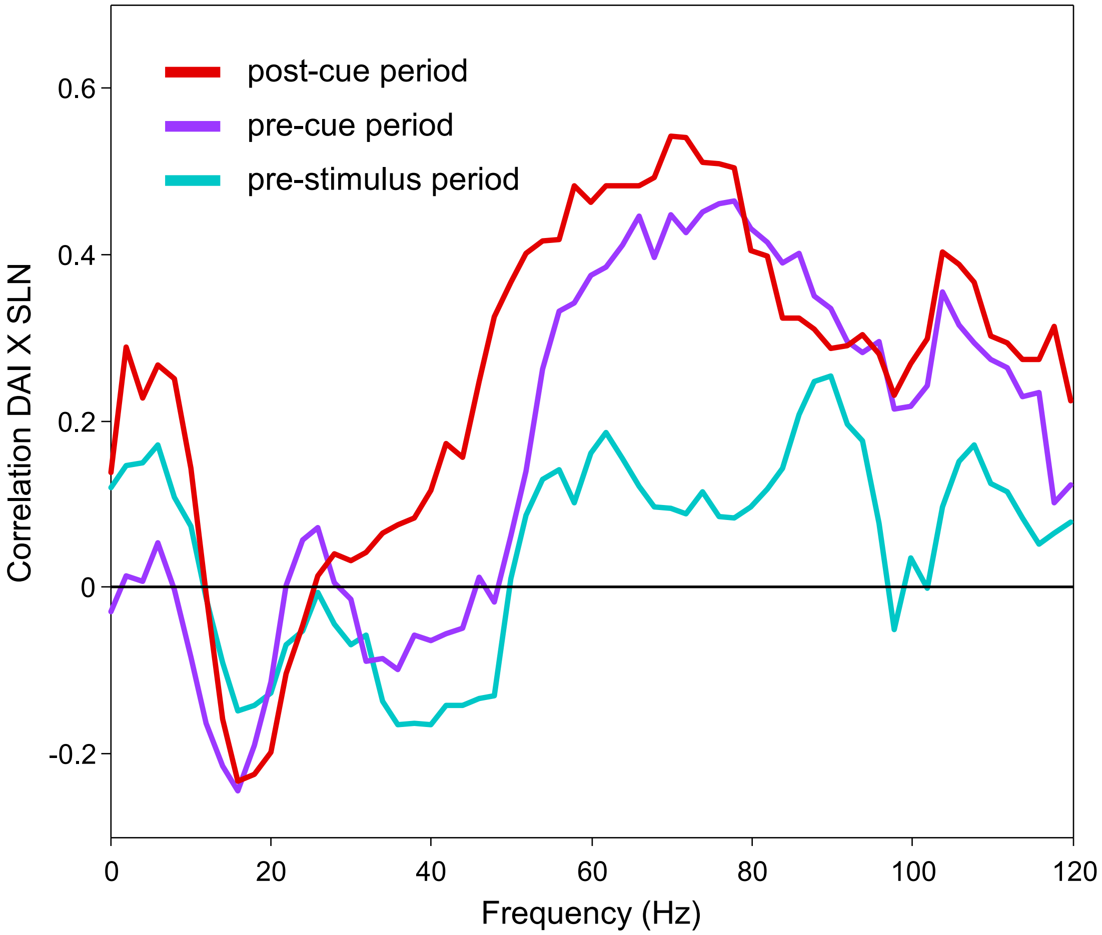

Extended Data Figure 5

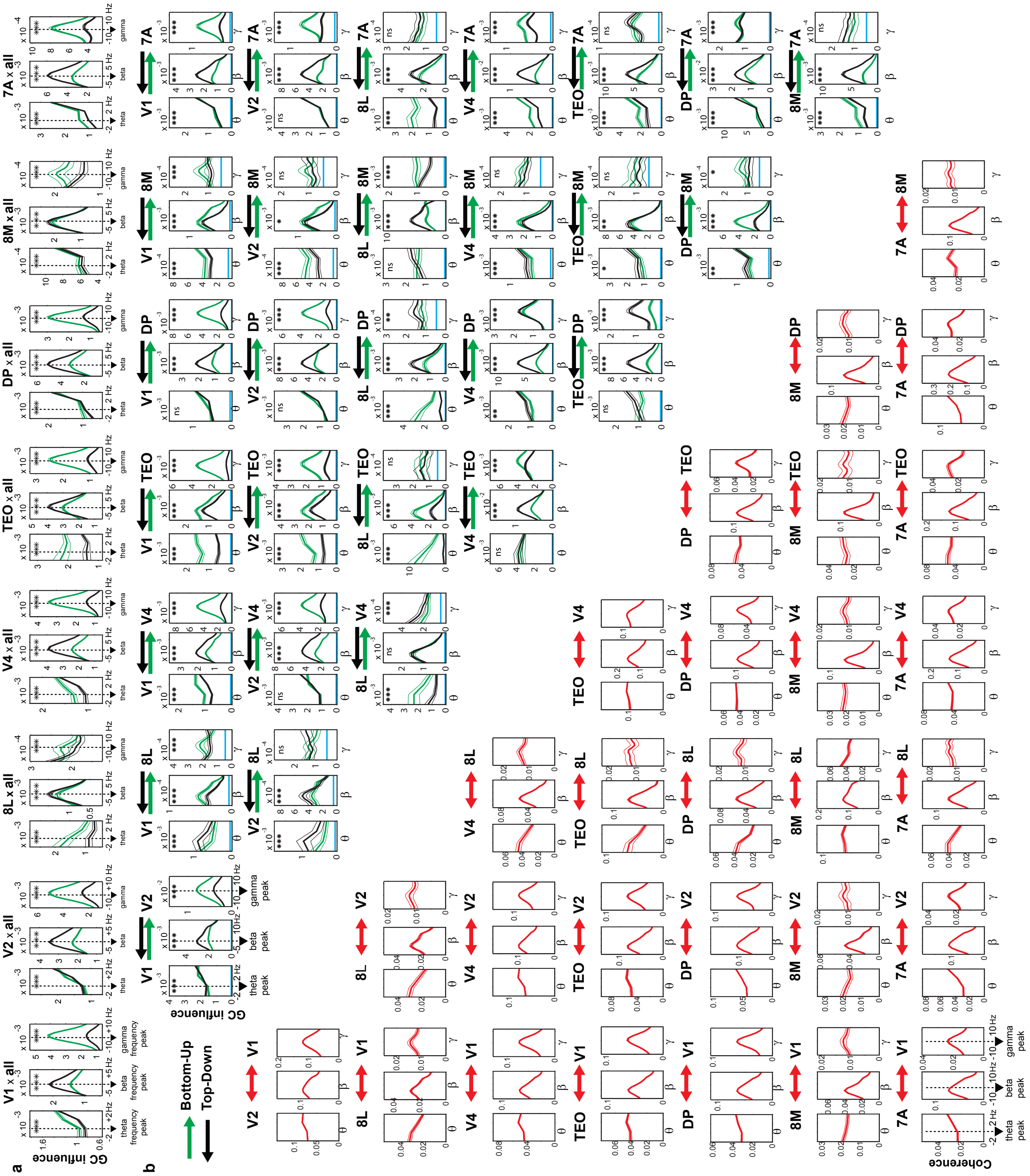

Extended Data Figure 6

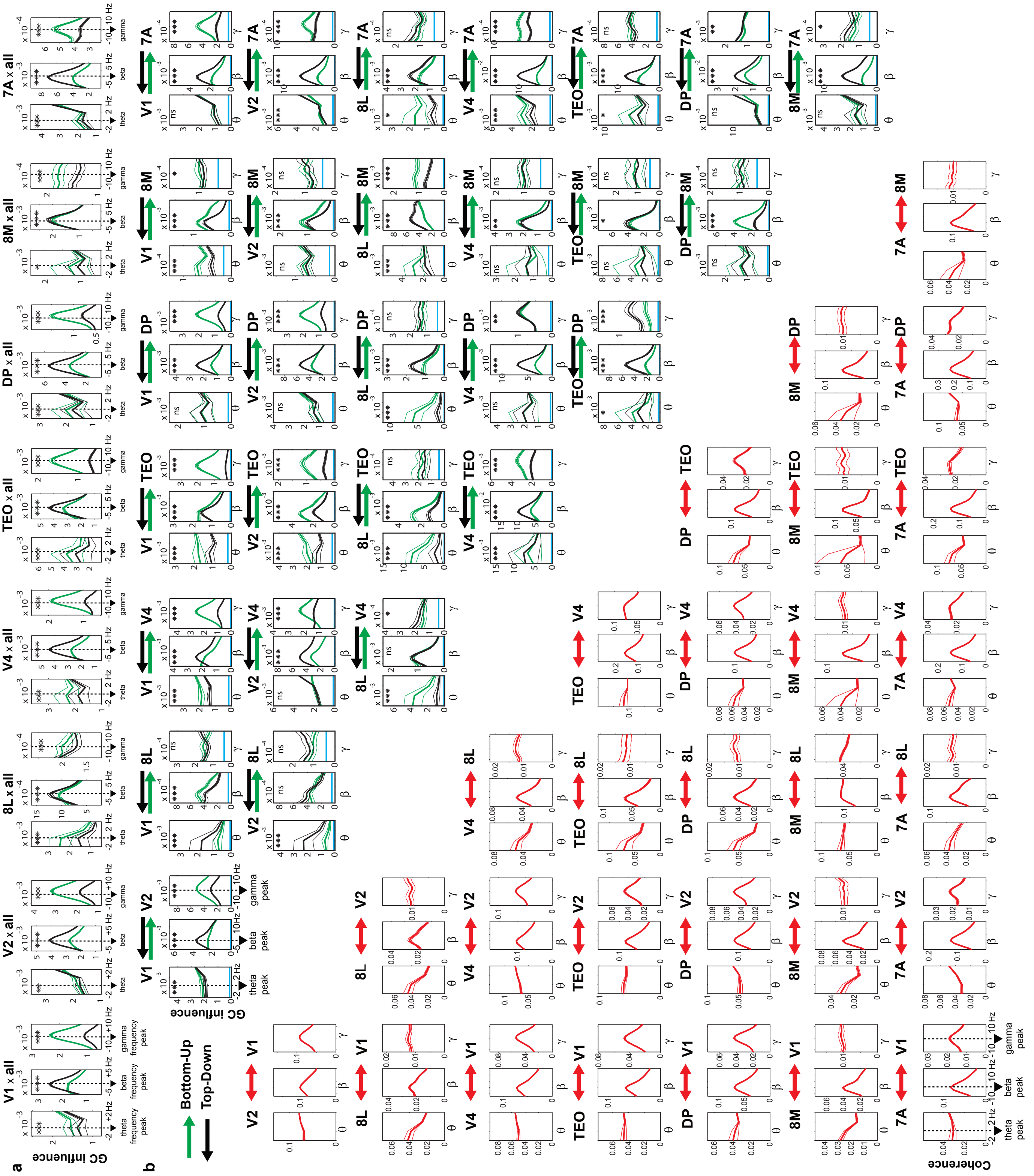

Extended Data Figure 7

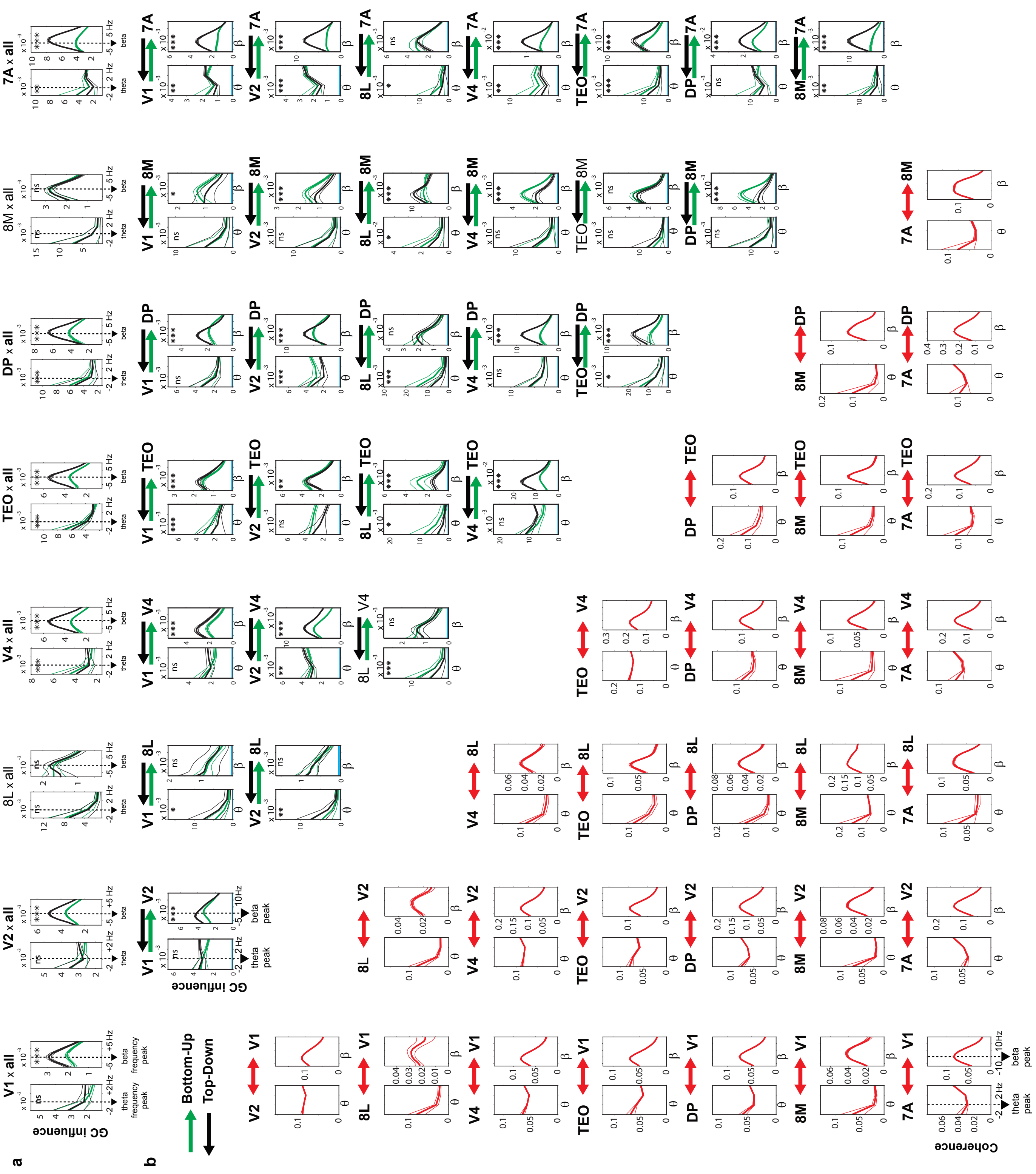

Extended Data Figure 8

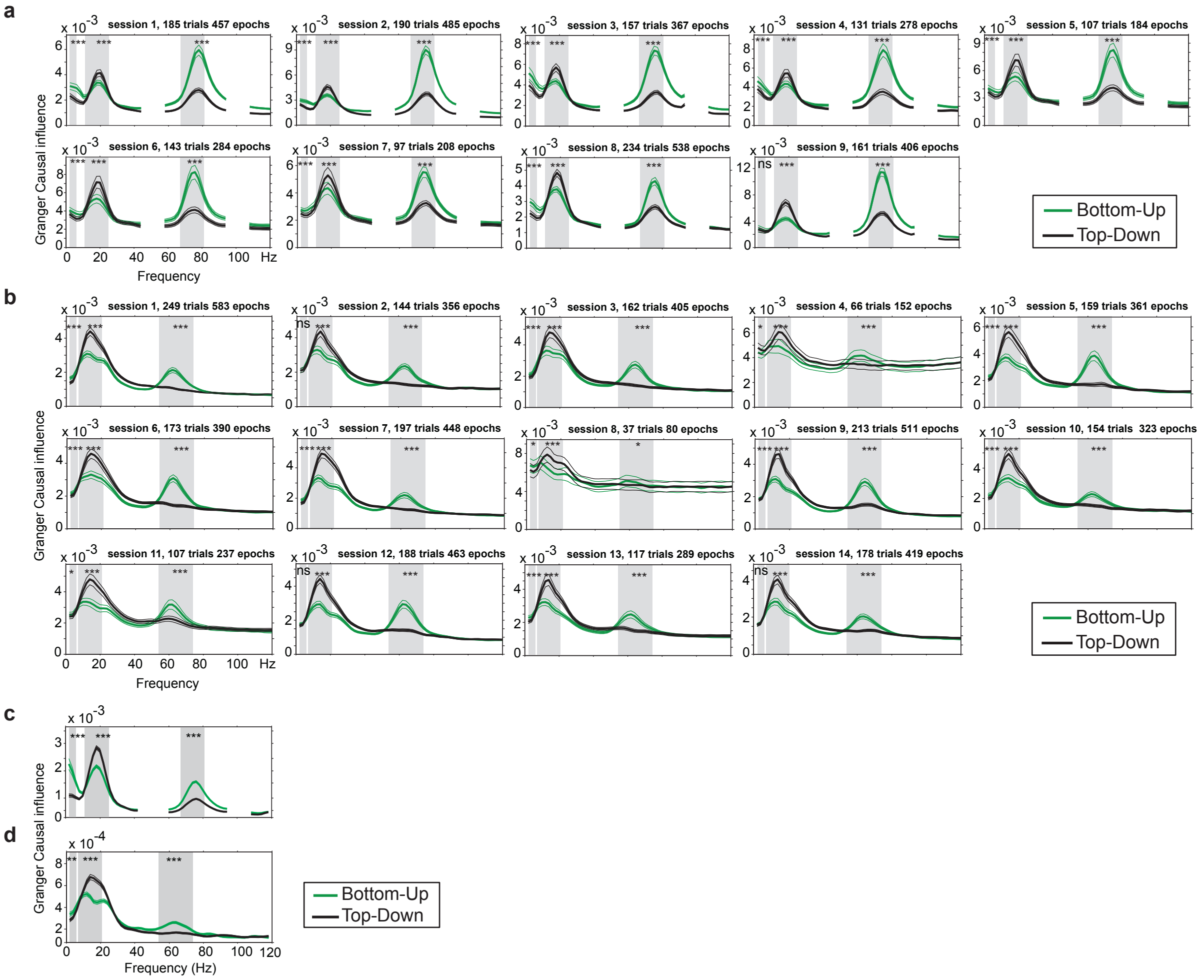

Extended Data Figure 9

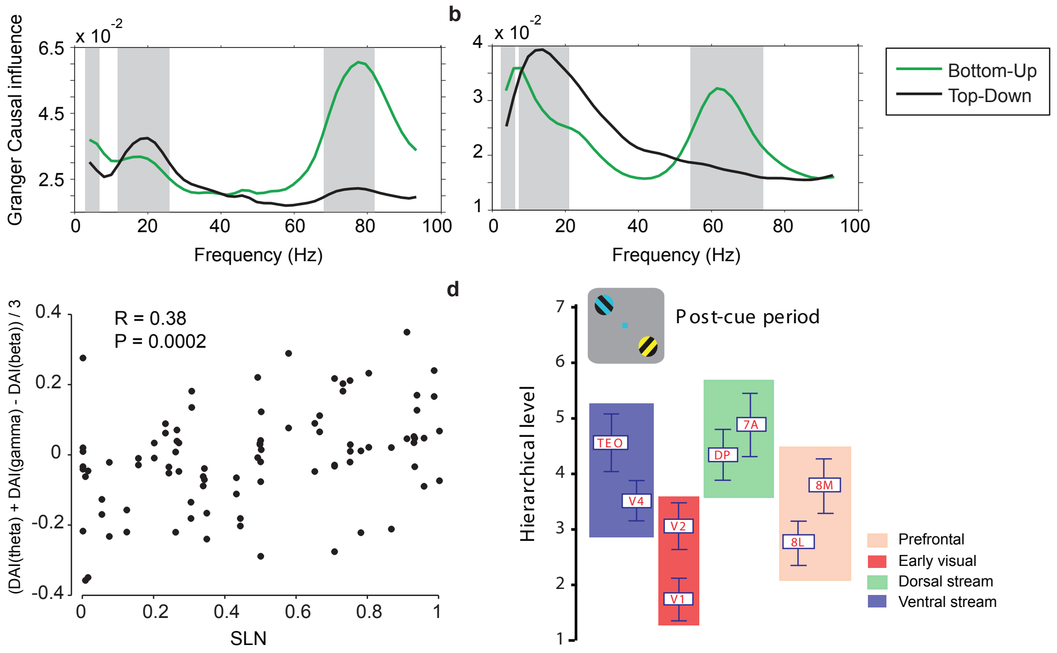

Extended Data Figure 10